MIL, SIL and PIL Implementation for Closed Loop Control of Flyback Converter

Muhammad ALI[1] , Ismet SEN[1] , Salih Baris OZTURK[1] , Emre AVCI[2,*]

[1]Istanbul Tech. Uni., Dep. of Electrical Engineering, 34469 Maslak, Istanbul, Türkiye
[2] Duzce Uni., Dep. of Electrical and Electronics Engineering, 81620, Duzce, Türkiye

Highlights
• MIL, SIL, and PIL enable rapid development of control algorithms for flyback converters.
• Validation of control algorithms through MIL, SIL, and PIL techniques enhances performance.
• MIL, SIL, and PIL techniques accelerate the design cycle of flyback converter control systems.

Abstract

Power electronic systems are rapidly evolving; thus, effective prototyping methods are required to test control algorithms and assess system performance prior to hardware implementation. This research suggests a Model-In-The-Loop (MIL), Software-In-The-Loop (SIL), and Processor-In-The-Loop (PIL) methodologies-based complete prototyping strategy for flyback converters using the TI F28069M Launchpad kit. These techniques can be combined to evaluate control strategies accurately and quickly, speeding up design cycles and enhancing system reliability. The proposed prototyping platform is presented in this work, along with a thorough explanation of each prototyping stage and its associated advantages. The effectiveness of the suggested approach for 50W rated power flyback converter in terms of quick algorithm development, system simulation, real-time control implementation and controller design accuracy is analyzed and shown by experimental results. The results show that the performance of the designed controller for the flyback converter is almost the same as in MIL and SIL implementation in terms of the overshoot and settling time in the reference voltage tracking. On the other hand, in the PIL implementation, the overshoot performance of the controller deviates by 1.18% more than in SIL and MIL implementation. These also confirm that the flyback control system's performance is reliable and effective during all phases of development.

1. INTRODUCTION

Modern electrical energy conversion heavily relies on power electronic systems, which find extensive applications in electrical transportation applications, industrial automation, and renewable energy systems [1-3]. The accurate design of control algorithms for these systems plays a crucial role in achieving optimal performance. Particularly, the control of flyback converters demands precision and efficiency due to their widespread usage in various application areas [4, 5].

Flyback converters are widely employed in applications where galvanic isolation and voltage regulation are essential. They are commonly used in power supplies, battery charging systems, LED drivers, and other low-to-medium power applications [6-8]. The design of an effective and accurate controller for flyback converters is paramount to ensure stable operation, efficient energy conversion, and reliable performance.

In the realm of control algorithm development for power electronic systems, historical approaches often involved time-consuming and expensive hardware prototyping. This traditional process necessitated the construction of physical prototypes, the implementation of control algorithms on specialized

*Corresponding author, e-mail: emreavci@duzce.edu.tr

microcontrollers or DSPs, and extensive laboratory testing to evaluate their performance. However, such conventional methods face challenges in terms of time-to-market, design flexibility, and cost.

To address these challenges, rapid control prototyping (RCP) techniques have gained popularity in recent years as efficient procedures for accelerating the development of power electronics systems [9-12]. RCP enables designers to validate control algorithms and assess system performance in a virtual environment before committing to hardware implementation. This paradigm shift significantly reduces development time and mitigates the risks of errors and flaws during the hardware testing phase.

This paper presents a comprehensive MIL, SIL and PIL implementation to develop an RCP process of control algorithms specifically tailored for flyback converters. By combining MIL, SIL, and PIL techniques, the proposed methodology enables efficient and accurate prototyping of flyback converter control systems. Leveraging the advantages of virtual simulations and real-time control execution, this approach greatly enhances the overall development process.

While real-time simulations are beneficial, their commercial versions often come with a high price tag, relying on specialized platforms with powerful computers and proprietary software. However, certain educational institutions and research facilities have established real-time simulators using more available technologies like DSPs and FPGAs to address this issue. Existing literature [13-18] showcases various alternative methods, such as utilizing external DSPs or CPUs for digital controllers, implementing power converter models on FPGAs, and leveraging multi-core processors for controlling analog/digital channels. These approaches demonstrate promising solutions for affordable simulation platforms that rely on widely accessible technology.

The subsequent sections of this paper provide a detailed exploration of the proposed RCP approach. Section 2 provides an overview of flyback converters and highlights their control requirements. Section 3 describes the proposed MIL, SIL and PIL platforms, emphasizing the integration of them to the flyback converter. Section 4 presents the controller design specifically tailored for flyback converters. Section 5 presents experimental results and performance evaluations, demonstrating the effectiveness of the proposed method. Lastly, Section 6 brings the work to a close by summarizing the results and outlining prospective future research trajectories.

2. ANALYZING THE DYNAMICS AND EFFICIENCY OF FLYBACK CONVERTER

2.1. Flyback Converter Principle

The flyback converter functions by facilitating energy transfer between the primary and secondary windings of a transformer. Figure 1 shows the schematic of a flyback converter.
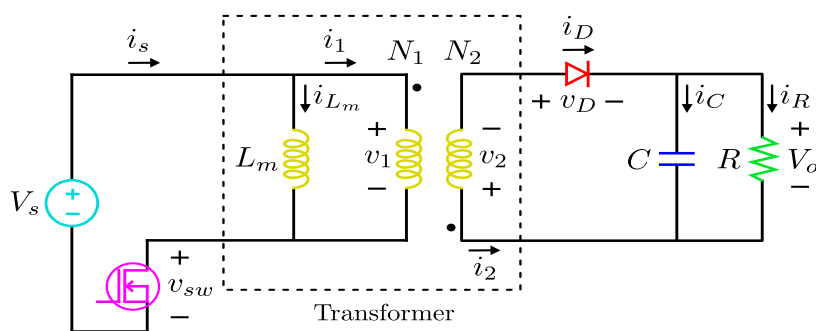
Figure 1. *Schematic of a flyback converter*

The key components of the circuit include a power switch (usually a MOSFET), a diode, a transformer, an energy storage element (inductor), and an output capacitor. Figure 2 shows the schematic of a flyback converter when the switch is closed.
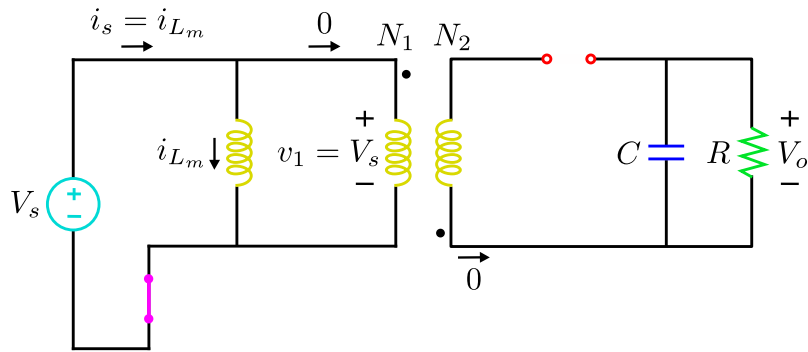
***Figure 2.** Schematic of a flyback converter when the switch is closed*

Analysis for the Switched Closed: The voltage across the magnetizing inductance, which is the voltage across the transformer primary winding, equals the source voltage (Figure 2). This is expressed in (1)

$$v_1 = V_s = L_m \frac{di_{L_m}}{dt} \tag{1}$$

where V_s is the source voltage, v_1 is the voltage across the primary side of the transformer, L_m is the magnetizing inductance, i_{L_m} is the magnetizing current.

The rate of change in the magnetizing current is obtained as in (2) by rearranging (1)

$$\frac{di_{L_m}}{dt} = \frac{\Delta i_{L_m}}{\Delta t} = \frac{\Delta i_{L_m}}{DT} \frac{V_s}{L_m} \tag{2}$$

where D is the duty ratio and T is the switching period.

Using (2) as a starting point, the change in the magnetizing current while the switch is closed can be obtained as follows:

$$(\Delta i_{L_m})_{closed} = \frac{V_s DT}{L_m} \; . \tag{3}$$

The voltage across the secondary side of the transformer when the switch is closed can be found from the primary voltage and the turn ratio of the transformer, as expressed in (4):

$$v_2 = v_1 \left(\frac{N_2}{N_1}\right) = V_s \left(\frac{N_2}{N_1}\right) \; . \tag{4}$$

The reverse voltage across the diode is the sum of the output voltage and secondary voltage of the transformer, as shown in (5):

$$V_D = -V_o - V_s \left(\frac{N_2}{N_1}\right) < 0 \tag{5}$$

where v_2 is the voltage across the secondary side of the transformer, N_2/N_1 is the transformer turns ratio, V_D is the diode voltage, V_o is the output voltage.

Given that the diode is off, the current flowing through the secondary side of the transformer is zero. Thus, the current in the primary windings of the ideal transformer is also zero:

$$i_2 = 0 \tag{6}$$

$$i_1 = 0 \tag{7}$$

where i_1 and i_2 are the currents flowing through the ideal transformer's primary and secondary windings, respectively.

In the ideal transformer model, when the switch is closed, there is no current flowing through the transformer's windings. However, there is a gradual and linear rise in the current flowing through the primary winding, which is inversely proportional to the magnetizing inductance L_m. This behavior implies that no current flows in the secondary winding of the transformer, and at the same time, the current in the physical primary winding steadily increases in a linear manner. Figure 3 shows the schematic of a flyback converter when the switch is open.
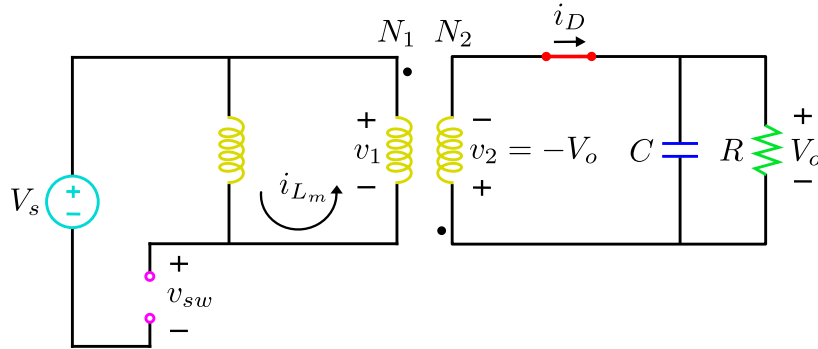
Figure 3. Schematic of a flyback converter when the switch is open

Analysis for the Switched Open: When the switch opens in Figure 3, the current in the inductance L_m cannot change instantly, necessitating a conduction path through the primary side turns of the ideal transformer. The current labeled as i_{L_m} enters through the undotted terminal of the primary winding and exits through the undotted terminal of the secondary winding. This arrangement is acceptable, given that the diode current is positive. The transformer's secondary voltage V_2 changes to $-V_o$ while maintaining a constant output voltage V_o. The voltage across L_m is established during the transformation back to the primary voltage from the secondary voltage

$$V_1 = -V_o \left(\frac{N_1}{N_2}\right). \tag{8}$$

For an open switch, the voltage across the secondary windings of the transformer is the negative output voltage since the diode is on:

$$v_2 = -V_o . \tag{9}$$

Then, the primary voltage is found from the turn ratio:

$$v_1 = v_2 \left(\frac{N_1}{N_2}\right) = -V_o \left(\frac{N_1}{N_2}\right). \tag{10}$$

The voltage across the magnetizing inductance equals the primary voltage. Then, the rate of change in the magnetizing current can be derived as in (11) and (12) based on (10)

$$L_m \frac{di_{L_m}}{dt} = v_1 = -V_o \left(\frac{N_1}{N_2}\right) \tag{11}$$

$$\frac{di_{L_m}}{dt} = \frac{\Delta i_{L_m}}{\Delta t} = \frac{\Delta i_{L_m}}{(1-D)T} = \frac{-V_o}{L_m} \left(\frac{N_1}{N_2}\right). \tag{12}$$

From (12), the variation in the transformer's magnetizing current when the switch is open can be determined as in (13):

$$(\Delta i_{L_m})_{open} = \frac{-V_o(1-D)T}{L_m}\left(\frac{N_1}{N_2}\right).$$ (13)

Since steady-state operation requires that the average change in the inductor current would be zero during a period, (14) applies:

$$(\Delta i_{L_m})_{closed} + (\Delta i_{L_m})_{open} = 0.$$ (14)

Substituting (3) and (13) into (14) gives (15):

$$\frac{V_s DT}{L_m} - \frac{V_o(1-D)T}{L_m}\left(\frac{N_1}{N_2}\right) = 0.$$ (15)

Solving (15) for V_o, the relation between the input and output voltages of the flyback converter is obtained to be:

$$V_o = V_s\left(\frac{D}{1-D}\right)\left(\frac{N_2}{N_1}\right).$$ (16)

The flyback converter shares a resemblance with buck-boost converters in terms of the input-output relationship. However, it incorporates the transformer ratio as an additional factor in its operation.

2.2. Flyback Converter Design

A flyback converter is designed to supply a resistive load while meeting the following specifications: the input voltage is 24 V, the output voltage is 48 V, and the output power is 50 W.

Let the duty ratio be

$$D = 0.4 .$$ (17)

Then, the transformer turns ratio is calculated in (18), which is derived based on (16):

$$\frac{N_2}{N_1} = \frac{V_o}{V_s}\left(\frac{1-D}{D}\right) = \frac{48}{24}\left(\frac{1-0.4}{0.4}\right) = 3.$$ (18)

The equivalent load resistance R is calculated from the output power P_o:

$$R = \frac{V_o^2}{P_o} = \frac{48^2}{50} = 46.08 \ \Omega .$$ (19)

The average current in L_m is

$$I_{L_m} = \frac{V_o}{(1-D)R}\left(\frac{N_2}{N_1}\right) = \frac{48}{(1-0.4)46.08}(3) = 5.208 \ A .$$ (20)

To provide a balance between the component sizes and the efficiency, the switching frequency f is selected arbitrarily as

$$f = 100 \ kHz .$$ (21)

Rearranging (3), the magnetizing inductance formula is obtained as in (22). Then, the required inductance value is calculated, assuming the current variation in L_m is 40% of the average current

$$L_m = \frac{V_s D}{\Delta i_{L_m} f} = \frac{24(0.4)}{0.4(5.208)(100,000)} = 46.08 \ \mu H .$$ (22)

The variation in the capacitor charge can be written as (23) from the integral of the capacitor current (output current) when the switch is on

$$|\Delta Q| = \left(\frac{V_o}{R}\right) DT = C\Delta V_o \;. \tag{23}$$

Then, the output capacitance expression is obtained as in (24), and the required capacitance value is calculated to make the output voltage ripple less than 0.5 percent:

$$C = \frac{D}{R(\Delta V_o/V_o)f} = \frac{0.4}{46.08(0.005)(100{,}000)} = 17.36 \; \mu F \;. \tag{24}$$

3. MIL, SIL AND PIL PLATFORMS FOR THE RCP PROCESS

In this section, being a part of the RCP process, the MIL, SIL, and PIL methodologies are detailed. Integration of these methodologies enables efficient and accurate prototyping of control algorithms for flyback converters.

3.1. Model-In-The-Loop (MIL) Technique

The basis of our pre-RCP platform relies on the MIL technique, which entails constructing an average model to portray the dynamic behavior of the flyback converter. The model encompasses both the power electronics circuitry and the control algorithm. We utilize MATLAB®/Simulink® to construct this comprehensive model, considering the converter's electrical characteristics, switching dynamics, and control strategy.

By utilizing the MIL technique, we can evaluate the control algorithm's performance in a simulated environment. This allows for quick iterations and fine-tuning of the algorithm parameters without the need for hardware implementation. We can simulate various operating conditions and evaluate the converter's response to load changes, input voltage variations, and other disturbances. This early-stage validation provides valuable insights into the control algorithm's effectiveness and robustness. Figure 4 shows the Model-In-The-Loop scheme for the closed-loop control of a flyback converter. The plant model and the controller model are illustrated in Figure 4.
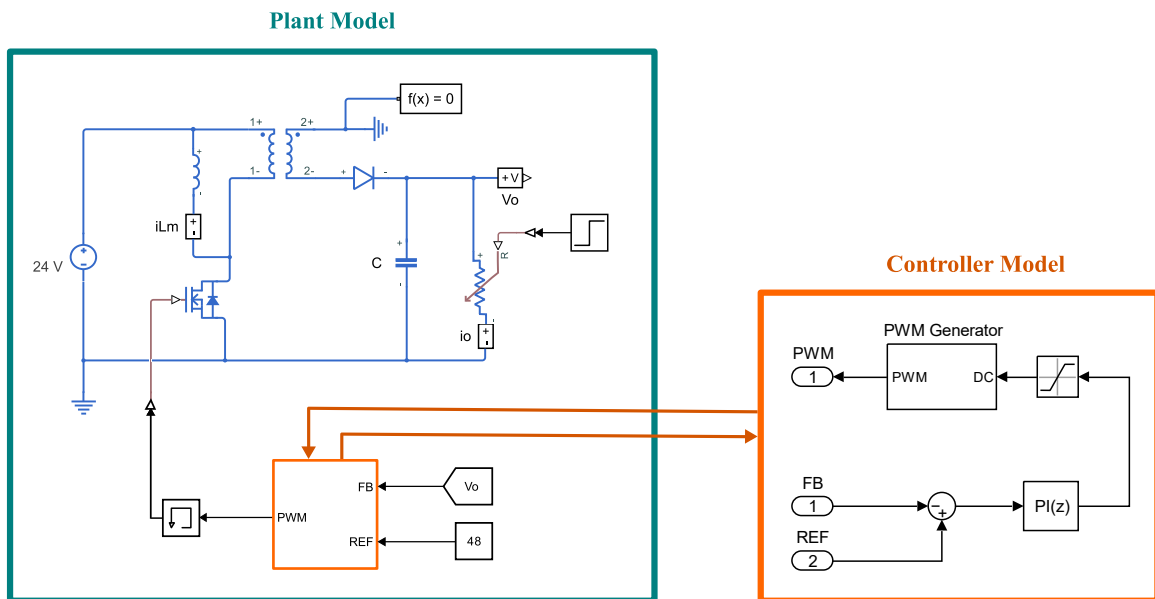
Figure 4. *MIL scheme for the closed-loop control of a flyback converter*

3.2. Software-In-The-Loop (SIL) Technique

Once the control algorithm has been refined and validated in the MIL stage, we proceed to the SIL technique. In this phase, the control algorithm is implemented in real-time software, typically using MATLAB®/Simulink®'s embedded code generation tools. Figure 5 shows the Software-In-The-Loop scheme for the closed-loop control of a flyback converter. Figure 5 illustrates the plant model and its integration with C Code on the host computer.
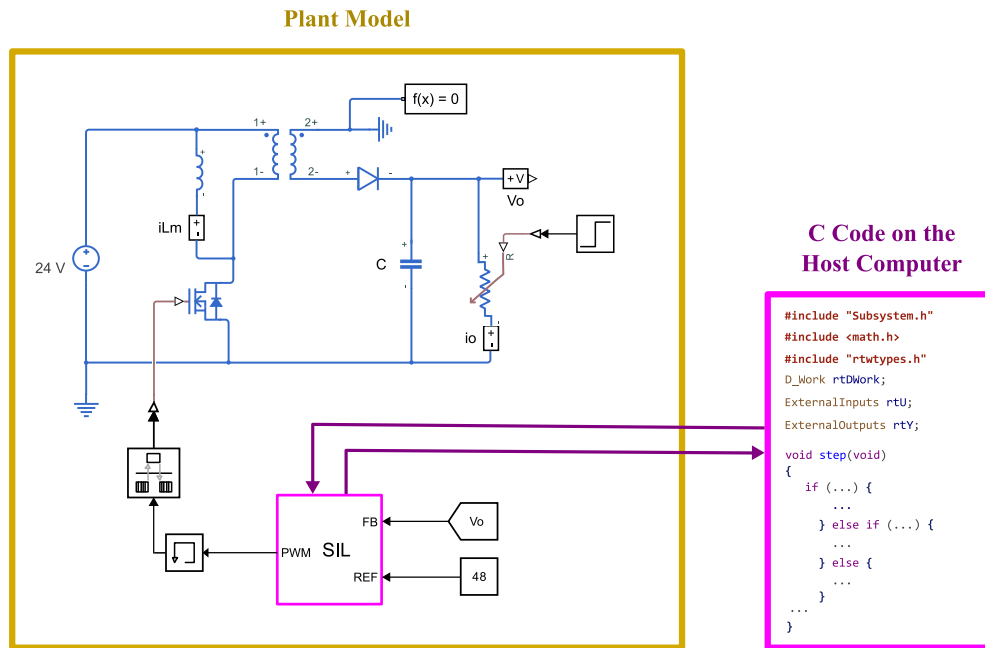
Figure 5. *SIL scheme for the closed-loop control of a flyback converter*

After generating the code, it is executed on a host computer to simulate the behavior of the control algorithm. This emulation mimics the execution on a dedicated microcontroller or DSP, such as the TMS320F28069M launch pad kit used in our case. Through the SIL technique, we can evaluate the real-time performance of the control algorithm within a simulated hardware environment. By connecting the control algorithm model to the flyback converter model, we can evaluate the control algorithm's behavior under realistic operating conditions. This includes considerations for signal conditioning, timing delays, and any non-idealities associated with the hardware implementation.

The SIL technique provides valuable insights into the control algorithm's computational requirements, response times, and stability. It allows us to assess the feasibility and efficiency of the algorithm in real-time execution, ensuring that it meets the stringent performance criteria required for power electronic systems.

3.3. Processor-In-The-Loop (PIL) Technique

The final stage of our pre-RCP platform involves the PIL technique. In this phase, the control algorithm is implemented on a TMS320F28069M launch pad kit, which interfaces with the flyback converter implemented in MATLAB®/Simulink®. The microcontroller or DSP serves as the real-time controller, executing the control algorithm and providing closed-loop feedback control.

The PIL technique allows us to assess the control algorithm's performance in a real-world hardware environment. By connecting the control algorithm to the physical system, we can evaluate its response to actual load variations, input voltage fluctuations, and other environmental factors. This enables us to validate the algorithm's effectiveness, robustness, and stability under realistic operating conditions. Figure 6 shows the Processor-In-The-Loop scheme for the closed-loop control of a flyback converter.

Furthermore, the PIL technique facilitates HIL testing, where the control algorithm is subjected to various fault conditions and system disturbances. This helps identify potential issues and ensures the algorithm's resilience in the face of unexpected events.

By integrating the MIL, SIL, and PIL techniques, our pre-RCP platform provides a comprehensive and efficient approach to the development and validation of control algorithms for flyback converters. It enables designers to iterate through various control strategies, optimize parameters, and evaluate system performance before completing the full RCP process.
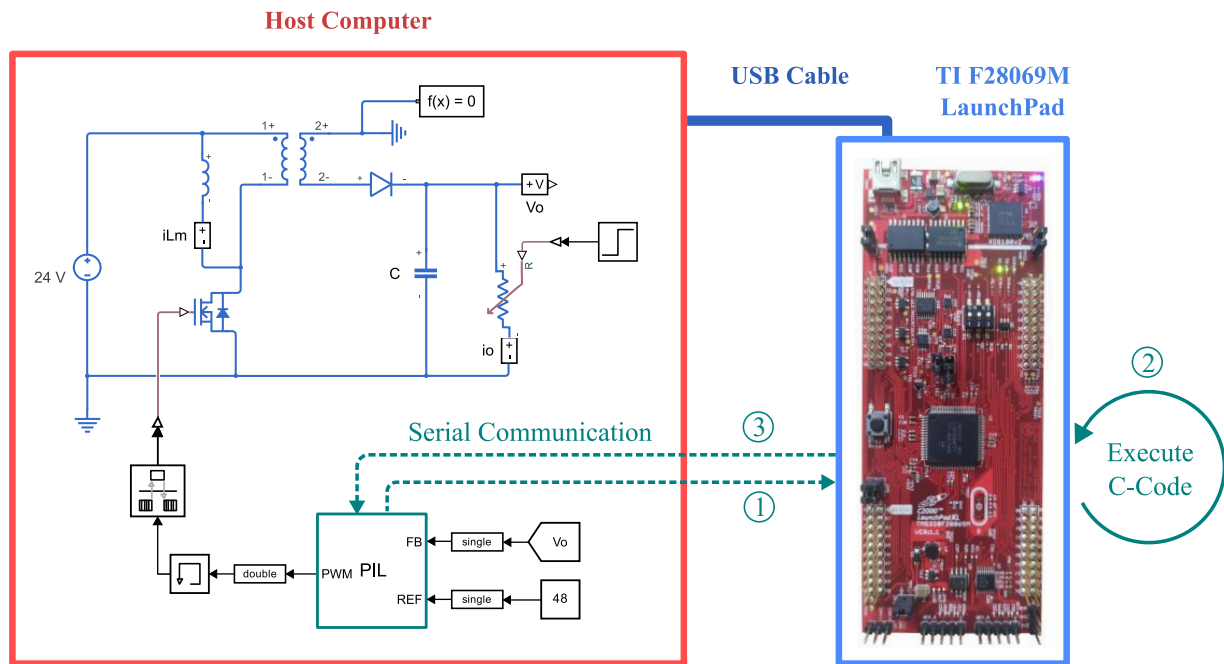
Figure 6. *PIL scheme for the closed-loop control of a flyback converter*

4. CONTROLLER DESIGN FOR FLYBACK CONVERTER

The procedure for designing a digital PI controller specifically for the flyback converter is explained. The controller design employs average-model-based autotuning to determine the appropriate PI parameters. Before delving into the details of the controller design, the circuit parameters of the developed flyback converter are presented. To assess the stability of the proposed controller, the open-loop transfer function of the system is used for bode plotting. Figure 7 shows the closed-loop control scheme of a flyback converter.
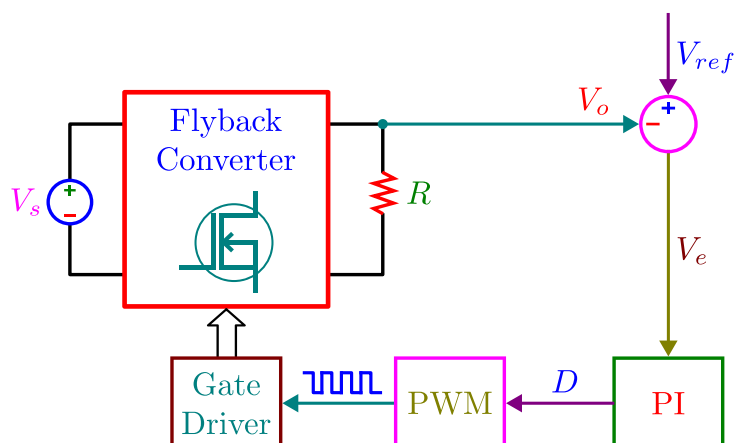
Figure 7. *The closed-loop control scheme of a flyback converter*

The circuit parameters of the flyback converter are shown in Table 1. The first three of these parameters are the converter's design specs, and the rest are determined according to the flyback converter design process given in Section 2.2.

Table 1. Circuit parameters of the flyback converter

Parameter	Symbol	Value	Unit
Input voltage	V_s	24	V
Output voltage	V_o	48	V
Output power	P_o	50	W
Duty cycle	D	0.4	-
Transformer turns ratio	N_2/N_1	3	-
Load resistance	R	46.08	Ω
Switching frequency	f	100	kHz
Magnetizing inductance	L_m	46.08	µH
Filter capacitance	C	17.36	µF

4.1. Autotuning of PI Parameters Based on the Average Model

MATLAB$^{®}$/Simulink$^{®}$'s PID Tuner enables easy and fast tuning of the PI controller parameters. However, the controlled plant model has to be suitable for linearization to enable the implementation of this automated tuning method. Since the switched model of a power electronics converter cannot be linearized, it is necessary to use the average model of the flyback converter during the autotuning process. For that purpose, the average model is developed for the continuous conduction mode (CCM) of the flyback converter based on [19] as in the following procedure:

The instantaneous values of switch current (i_{sw}) and diode voltage (v_D) are expressed as:

$$i_{sw} = \begin{cases} i_{Lm}, & 0 < t < DT_s \\ 0, & DT_s < t < T_s \end{cases} \tag{25}$$

$$v_D = \begin{cases} -\dfrac{N_2}{N_1} v_s - v_o, & 0 < t < DT_s \\ 0, & DT_s < t < T_s \end{cases} \tag{26}$$

where T_s denotes the switching period. Then, the average switch current ($\overline{i_{sw}}$) and diode voltage ($\overline{v_D}$) can be derived as:

$$\overline{i_{sw}} = \frac{1}{T_s}\int_0^{T_s} i_{sw} dt = \frac{1}{T_s} i_{Lm} DT_s = \boldsymbol{Di_{Lm}} \tag{27}$$

$$\overline{v_D} = \frac{1}{T_s}\int_0^{T_s} v_D dt = \frac{1}{T_s}\left(-\frac{N_2}{N_1} v_s - v_o\right) DT_s = -\frac{\boldsymbol{N_2}}{\boldsymbol{N_1}} \boldsymbol{Dv_s} - \boldsymbol{Dv_o}. \tag{28}$$

To create the average model, these equations are used as dependent sources, and the switch and diode in the flyback converter are substituted. Figure 8 shows the average model's circuit diagram.
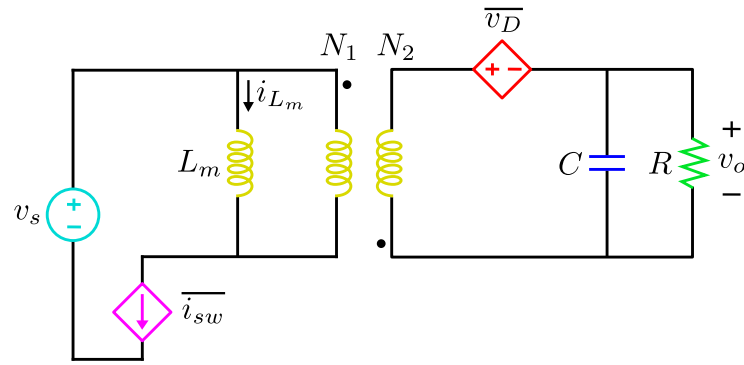
Figure 8. *Average model of the flyback converter*

The average model of the flyback converter is constructed in MATLAB®/Simulink®. The control-to-output voltage transfer function of the system is obtained from the linear analysis of the Simulink® model and given in (29)

$$P(s) = \frac{V_o(s)}{D(s)} = \frac{0.0004608s + 10^{10}}{s^2 + 1250s + 1389(10)^8} \ . \tag{29}$$

The PI controller is included in that Simulink® model to adjust the duty cycle (D) based on the output voltage (V_o) feedback. Then, the "autotuning" of the PI parameters is performed using the PID Tuner, and the results are presented in Table 2.

Table 2. *Autotuned PI parameters in MATLAB®/Simulink®*

Name	Symbol	Value
Proportional constant	K_p	0
Integral constant	K_i	2.3379

The transfer function of the controller is given in (29)

$$C(s) = \frac{D(s)}{V_e(s)} = K_p + \frac{K_i}{s} = \frac{2.3379}{s} \ . \tag{30}$$

Then, the open-loop transfer function of the control system $G_{ol}(s)$ is found as in (31)

$$G_{ol}(s) = \frac{V_o(s)}{V_e(s)} = C(s)P(s) = \frac{0.001077s + 2.338(10)^{10}}{s^3 + 1250s^2 + 1389(10)^8 s} \ . \tag{31}$$

The bode plot of $G_{ol}(s)$ is given in Figure 9. It is shown that the gain margin (GM) is 17.4 dB (at 11.8 krad/s) and the phase margin (PM) is 89.9 degrees (at 168 rad/s). Since both the GM and PM are positive, the developed feedback control system is stable.
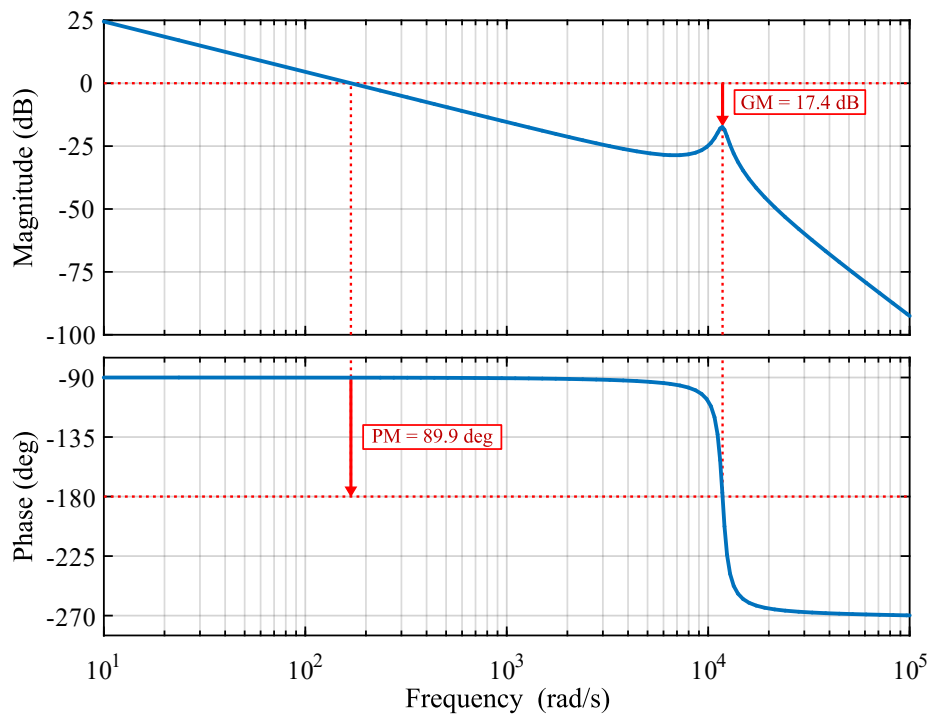
***Figure 9.** Bode plot of the open-loop transfer function of the system with PI controller*

5. MIL, SIL, AND PIL SIMULATION RESULTS

In this section, the results of MIL, SIL, and PIL simulations are presented, discussed, and compared with each other. As the first stage of the proposed methodology, a MIL simulation is performed in MATLAB®/Simulink® to assess the developed PI controller's performance in controlling the switched model of the flyback converter. The converter is started at full load, and after it reaches the steady state, a step change in the load is applied to half its value. Then, the transient state is observed to better examine the dynamic behavior of the control algorithm. The output voltage and output current waveforms obtained from the MIL simulation are given in Figures 10 and 11.
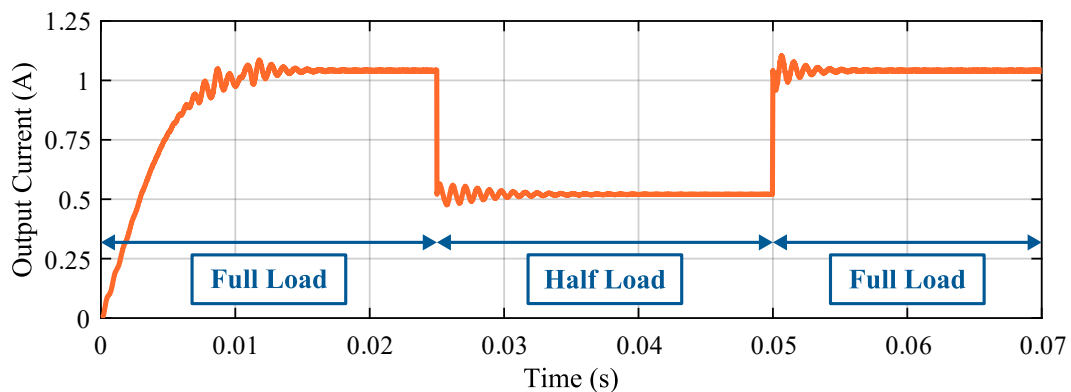
***Figure 10.** Output current from the MIL simulation*
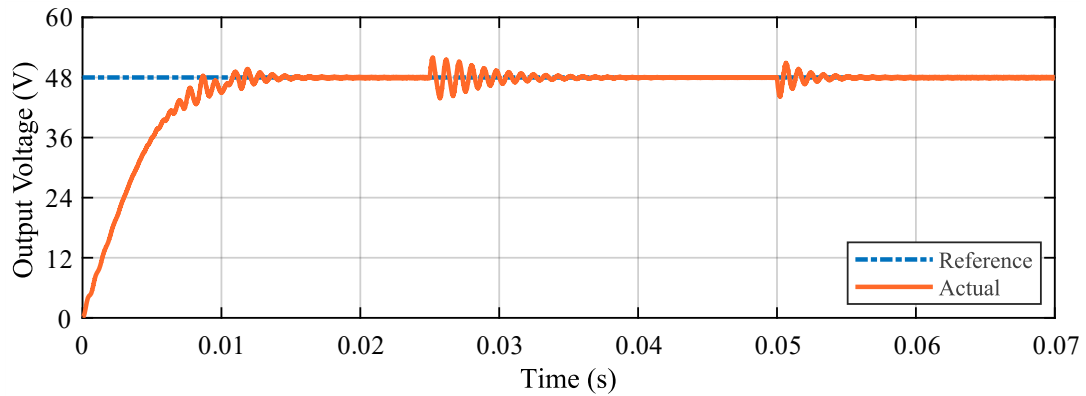
Figure 11. Output voltage from the MIL simulation

The MIL simulation results clearly demonstrate the devised control algorithm's acceptable performance in terms of both steady-state and transient behavior. The output voltage settles down to the desired level of 48 V with the settling time and maximum overshoot values given in Table 3.

In the next stage, the automatic code generation is performed on the MATLAB®/Simulink® platform, and a SIL test is carried out for the validation of the generated code. The resultant waveforms of output current and voltage are presented in Figures 12 and 13.
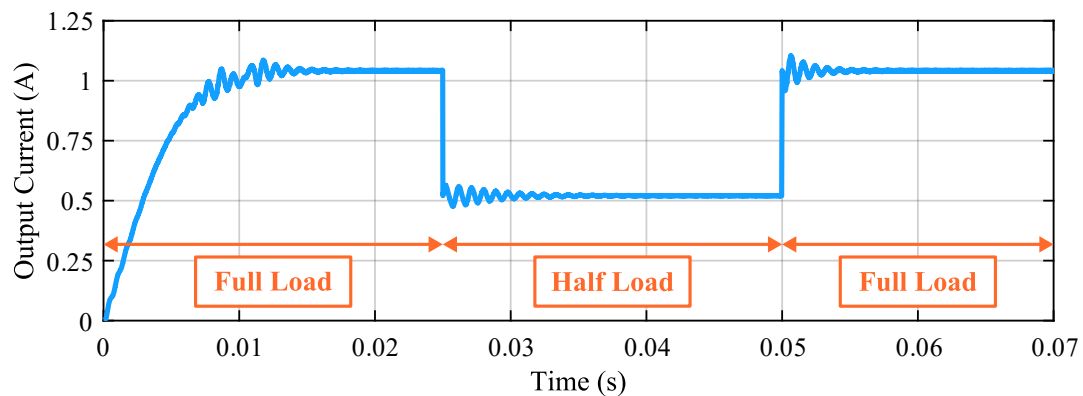
Figure 12. Output current from SIL test
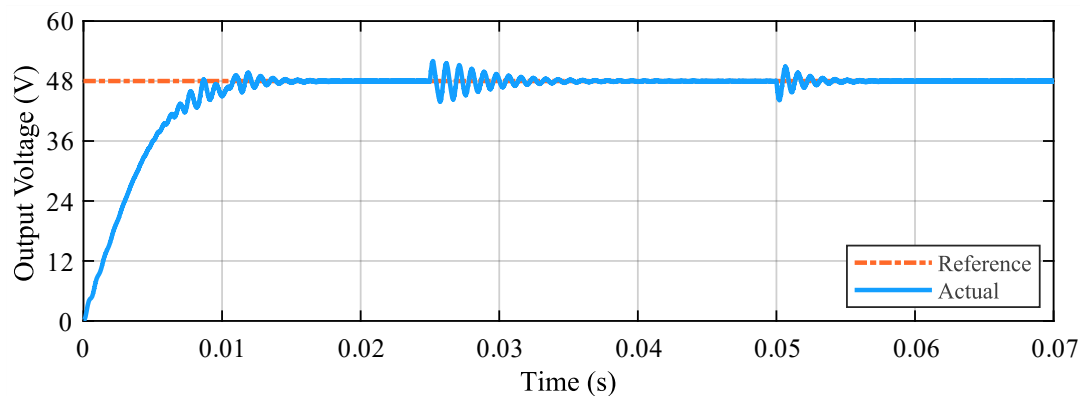
Figure 13. Output voltage from SIL test

The simulation results obtained from the SIL test perfectly match the results of the MIL simulation without any errors, which verifies the successful code generation and the proper operation of the generated code.

As the last step of RCP, a PIL test is performed to evaluate the execution of the autogenerated C code on the target hardware (TI F28069 Launchpad). The output current and output voltage plots are given in Figures 14 and 15. The output voltage waveform obtained from the PIL simulation is differentiate with that of the MIL and SIL in Figure 16.
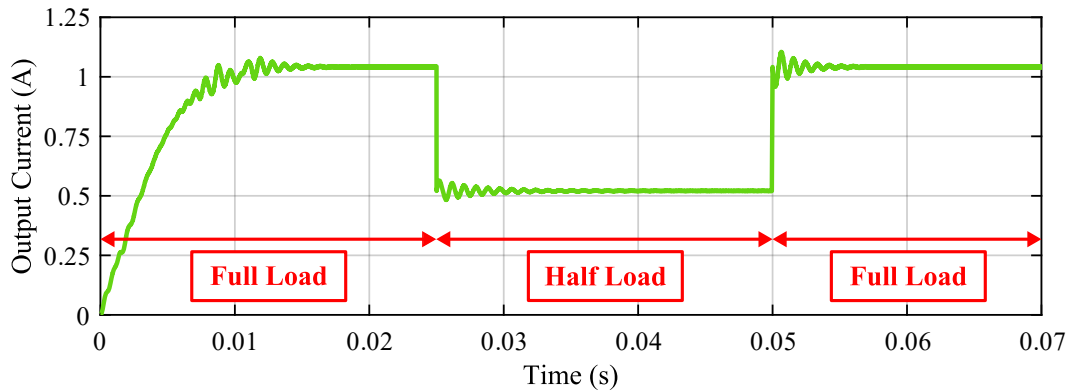
Figure 14. *Output current from PIL test*
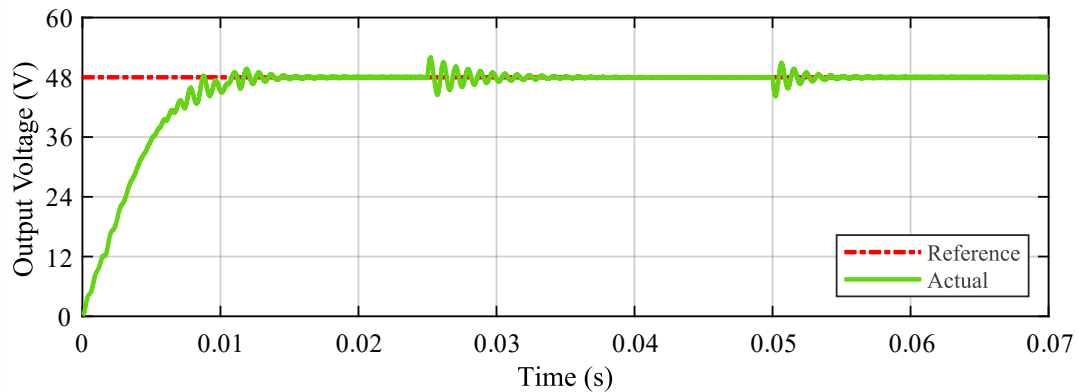
Figure 15. *Output voltage from PIL test*
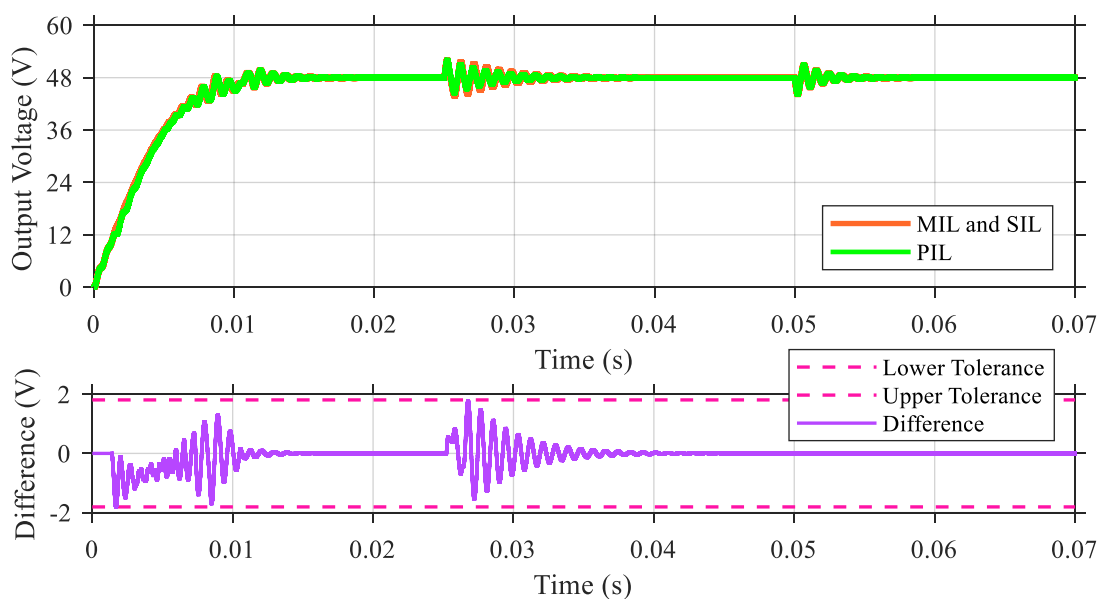
Figure 16. *Comparison between the results of MIL, SIL, and PIL*

Figure 16 clearly demonstrates how closely the outcomes of the PIL simulation match those of the MIL and SIL simulations. The absolute error between two output voltage waveforms does not exceed 1.81 V, which is only 3.77% of the steady-state value. The settling time and maximum overshoot values in case of MIL, SIL, and PIL simulations are presented in Table 3 for comparison.

Table 3. Comparison of transient response specifications under MIL, SIL, and PIL tests

Parameter	Symbol	Pre-RCP Stages		
		MIL	SIL	PIL
Maximum overshoot (%)	M_p	3.552	3.552	3.594
Settling time for 2% (ms)	t_s	12.82	12.82	12.83

The transient response specifications of the feedback control system obtained from the MIL and SIL simulations are exactly the same, and they are very close to the results of the PIL. The maximum overshoot obtained from the PIL test deviates 1.18% from the MIL and SIL results, and the deviation is only 0.01 ms (0.078%) for the settling time.

In short, the results from MIL, SIL, and PIL simulations verify the satisfactory performance of the developed control algorithm and the successful execution of the autogenerated C code on the target hardware.

6. CONCLUSION

This article presents a comprehensive pre-RCP strategy for the development and testing of control algorithms specifically tailored for flyback converters. The proposed approach combines Model-In-The-Loop (MIL), Software-In-The-Loop (SIL), and Processor-In-The-Loop (PIL) techniques to enable efficient and accurate prototyping. The importance of RCP in the quickly developing field of power electronic systems is highlighted in the essay. Historically, the creation of control algorithms required time-consuming and expensive hardware prototyping, which created issues with time-to-market, design flexibility, and cost. However, before hardware implementation, RCP techniques have proven to be effective ways to validate control algorithms and evaluate system performance. In this work, the MIL, SIL and PIL techniques are analyzed for the controller design of the flyback converter. The experimental results show the effectiveness of the proposed approach, showing more consistent and reliable performance of PIL implementation across the other pre-RCP methods. The PIL test showed minimal deviations, with only a 1.18% difference in maximum overshoot and a mere 0.078% discrepancy in settling time compared to the MIL and SIL outcomes. These results confirm that the control system's performance was reliable and effective during all phases of development.

CONFLICTS OF INTEREST

No conflict of interest was declared by the authors.

REFERENCES

[1] Bose, B.K., Power electronics in renewable energy systems and smart grid: technology and applications, First Edition, New Jersey, (2019).

[2] Jahns, T.M., and Blasko, V., "Recent advances in power electronics technology for industrial and traction machine drives", Proceedings of the IEEE, 89(6): 963-975, (2001).

[3] Abu-Rub, H., Malinowski, M., and Al-Haddad, K., Power electronics for renewable energy systems, transportation and industrial applications, First Edition, West Sussex, (2014).

[4]   Venkatesan, K., "Current mode controlled bidirectional flyback converter", 20th Annual IEEE Power Electronics Specialists Conference, Milwaukee, 835-842, (1989).

[5]   Liang, T.J., Chen, K.H., and Chen, J.F., "Primary side control for flyback converter operating in DCM and CCM", IEEE Transactions on Power Electronics, 33(4): 3604-3612, (2017).

[6]   Mohammed, A.A., and Nafie, S.M., "Flyback converter design for low power application", International conference on computing, control, networking, electronics and embedded systems engineering (ICCNEEE), Khartoum, 447-450, (2015).

[7]   Bunyamin, T., and Kirimer, B., "An interleaved high-power flyback inverter for photovoltaic applications", IEEE transactions on Power Electronics, 30(6): 3228-3241, (2014).

[8]   Ponce-Silva, M., Salazar-Perez, D., Rodriguez, O.M., Vela-Valdes, L.G., Claudio-Sanchez, A., De Leon-Aldaco, S.E., Cortes-Garcia, C., Saavedra-Benitez, Y.I., Lozoya-Ponce, R.E., and Aqui-Tapia, J.A., "Flyback converter for solid-state lighting applications with partial energy processing", Electronics, 10(1): 60, (2020).

[9]   Ma, W., Chen, Y., and Yao, D., "PC-based real-time simulator and its application on testing of power plant auxiliary system control", 2010 International Conference on Power System Technology, Hangzhou, 1–4, (2010).

[10] Miyazaki, Y., Kimura, M., Karube, T., Noro, Y., Takahashi, C., Kishibe, H., and Sato, H., "Development and verification of a FACTS digital realtime simulator", IEEE/PES Transmission and Distribution Conference and Exhibition, Yokohama, 1: 324–329, (2002).

[11] Hercog, D., Curkovic, M., and Jezernik, K., "DSP based rapid control prototyping systems for engineering education and research", 2006 IEEE Conference on Computer Aided Control System Design, Munich, 2292-2297, (2006).

[12] Hao, X., Fu, L., Ma, F., and Li, C., "Real-time simulation hardware-in-the-loop test platform for DC integrated power system containing a large number of switches", IEEE 5th International Electrical and Energy Conference (CIEEC), Nangjing, 1600–1605, (2022).

[13] Ruelland, R., Gateau, G., Meynard, T.A., and Hapiot, J. -C., "Design of FPGA-based emulator for series multicell converters using co-simulation tools", IEEE Transactions on Power Electronics, 18(1): 455–463, (2003).

[14] Dufour, C., Lapointe, V., Bélanger, J., and Abourida, S., "Hardware-in-the-loop closed-loop experiments with an FPGA-based permanent magnet synchronous motor drive system and a rapidly prototyped controller", 2008 IEEE International Symposium on Industrial Electronics, Cambridge, 2152–2158, (2008).

[15] He, L., Wang, F., and Ke, D., "FPGA-based sliding-mode predictive control for PMSM speed regulation system using an adaptive ultralocal model", IEEE Transactions on Power Electronics, 36(5): 5784–5793, (2021).

[16] Zheng, J., Zhao, Z., Zeng, Y., Shi, B., and Yu, Z., "An event-driven real-time simulation for power electronics systems based on discrete hybrid time-step algorithm", IEEE Transactions on Industrial Electronics, 70(5): 4809–4819, (2023).

[17] Rodal, G.L., and Peftitsis, D., "Real-time FPGA simulation of high-voltage silicon carbide MOSFETs", IEEE Transactions on Power Electronics, 38(3): 3213–3234, (2023).

[18]   Mao, C., Leng, F., Li, J., Zhang, S., Zhang, L., Mo, R., Wand, D., Zeng, J., Chen, X., An, R., and Zhao, Y., "A 400-V/50-kVA digital–physical hybrid real-time simulation platform for power systems", IEEE Transactions on Industrial Electronics, 65(5): 3666–3676, (2018).

[19]   Akbarabadi, S.A., Atighechi, H., and Jatskevich, J., "Circuit-averaged and state-space-averaged-value modeling of second-order flyback converter in CCM and DCM including conduction losses", 4th International Conference on Power Engineering, Energy and Electrical Drives, İstanbul, 995-1000, (2013).